




# From micro to nano: polypropylene composites reinforced with TEMPO-oxidised cellulose of different fibre widths

Andre N. Gaduan · Laleh Solhi · Eero Kontturi · Koon-Yang Lee 

Received: 29 June 2020 / Accepted: 13 December 2020 / Published online: 11 February 2021  
© The Author(s) 2021

**Abstract** TEMPO-oxidised cellulose fibres are often explored as *nano*-reinforcement for polymers. However, it is unclear whether *micrometre-sized* TEMPO-oxidised cellulose fibres also possess similar reinforcing potential. In this work, we report the mechanical response of polypropylene (PP) composites reinforced with TEMPO-oxidised cellulose (TOC) of different fibre widths. *Micrometre-sized* TOC fibres (TOCF) containing sodium carboxylate (TOCF-Na) and free hydroxyl (TOCF-H) groups, as well as *nano-sized* TOC nanofibrils (TOCN) were produced from dissolving pulp and incorporated into PP matrix via melt-extrusion. It was found that model PP composites containing *micrometre-sized* TOCF-Na and TOCF-H possessed the highest tensile modulus of up to 2.5 GPa; 40% improvement over neat PP and 30% increase over PP/TOCN composite. No significant differences in the tensile strength of PP/TOCF-Na and PP/TOCF-H composites were observed when compared to neat PP. The incorporation of *nano-sized* TOCN into PP however, led to a 6% decrease in tensile strength. Single-edge notched beam fracture toughness test further showed that PP/TOCN

composite possessed the lowest fracture toughness of 2.52 MPa m<sup>1/2</sup>; a decrease of 18% over PP reinforced with *micrometre-sized* TOCF-Na and TOCF-H. Our study shows that *micrometre-sized* TOCFs serve as better reinforcement for polymers compared to *nano-sized* TOCN. This is attributed to the better dispersion of TOCF in the PP matrix. Furthermore, the presence of surface microfibrillation on TOCFs also enhanced the quality of the TOCF-PP interface through mechanical interlocking and local stiffening of the PP matrix.

**Keywords** Biocomposite · Nanocellulose · Pulp · Tensile properties · Extrusion

## Introduction

The publication of Chang and Robyt (1996), as well as the subsequently work by Isogai and Kato (1998) reported one of the first studies describing the selective oxidation of C6 hydroxyl groups of cellulose in water using catalytic amount of 2,2,6,6-tetramethylpiperidine-1-oxyl (TEMPO), with sodium hypochlorite (NaClO) and sodium bromide (NaBr) as the regenerating oxidants. The oxidation process introduces anionically charged carboxylate groups onto the surface of cellulose fibrils and this gives rise to strong electrostatic repulsions between the cellulose fibrils in water. Consequently, TEMPO-mediated oxidation of cellulose pulp allowed for the efficient individualisation of the cellulose fibrils to produce cellulose

A. N. Gaduan · K.-Y. Lee (✉)  
Department of Aeronautics, Imperial College London,  
South Kensington Campus, London SW7 2AZ, UK  
e-mail: koonyang.lee@imperial.ac.uk

L. Solhi · E. Kontturi  
Department of Bioproducts and Biosystems, Aalto  
University, P.O. Box 16300, 00076 Espoo, Finland

nanofibrils that possess uniform width and high aspect ratio at a relatively high yield using only minimal energy input (Saito et al. 2006). This simple method to produce cellulose nanofibrils has sparked a new wave of research into cellulose nanocomposites, particularly to explore TEMPO-oxidised cellulose nanofibrils (TOCN) as well as other cellulose-based nano-objects as reinforcement for polymers (Clarkson et al. 2020). The motivation behind utilising TOCN as nano-reinforcement is driven by the possibility of exploiting the high elastic modulus of cellulose crystals, estimated to be up to 160 GPa (Eichhorn and Davies 2006) and the high tensile strength of TOCN, measured to be between 2 and 6 GPa (Saito et al. 2013).

One of the earliest attempts to produce TOCN-reinforced polymer composites was reported by Johnson et al. (2009), who manufactured TOCN-reinforced hydropropylcellulose (HPC) with a TOCN loading fraction of 5 wt%. The composite was manufactured by dispersing TOCN in water with HPC dissolved, followed by solution casting and water evaporation. Whilst no quasi-static mechanical testing results were reported, dynamic mechanical analysis showed that TOCN-reinforced HPC composite possessed a storage modulus of  $\sim 2.5$  GPa at room temperature; a significant improvement over neat HPC of only  $\sim 1$  GPa. Numerous authors have since followed up the early work of Johnson et al. (2009) to explore TOCN as nano-reinforcement for various polymers, including polystyrene (Fujisawa et al. 2012), acrylonitrile-butadiene rubber (Fukui et al. 2018, 2019), poly(acrylamide) (Kurihara and Isogai 2014) and cellulose triacetate (Soeta et al. 2018) for the production of high performance optically transparent composite films, as well as poly(lactic) acid (Bulota et al. 2013; Hietala et al. 2014) to produce biocomposites with improved mechanical properties. High performance TOCN-reinforced poly(vinyl alcohol) fibres (Endo et al. 2013) and polypropylene composites (Wang et al. 2015) have also been produced.

Whilst the focus in recent literature has always been on the use of TOCN as *nano*-reinforcement, it is unclear whether *micrometre-sized* TEMPO-oxidised cellulose fibres (TOCF) that have not been mechanically disintegrated into TOCN could also serve as effective reinforcement for polymers. As the mechanical properties of a composite depend on both the quality of the fibre-matrix interface and the size of the reinforcing fibres (more accurately the surface area to

volume ratio) (Hull and Clyne 1996), the width of the TEMPO-oxidised cellulose fibres is anticipated to also play a governing role in the mechanical properties of the resulting composites. Therefore in this work, we report the effect of TEMPO-oxidised cellulose fibre width on the mechanical response of TEMPO-oxidised cellulose reinforced polypropylene (PP) composites. The tensile properties and fracture toughness of the resulting model PP composites are presented. This work also discusses the thermal degradation properties and viscoelastic behaviour of the model (TEMPO-oxidised) cellulose reinforced PP composites.

## Experimental

### Materials

Once-dried dissolving pulp derived from bagasse was kindly supplied by Guangdong Luzhou Paper Mould Packing Process Co. Ltd in the form of pressed pulp sheets (grammage =  $500 \text{ g m}^{-2}$ , bulk density =  $0.90 \pm 0.04 \text{ g cm}^{-3}$ ) and used as the cellulose source in this work. Chopped polypropylene fibres (diameter =  $20 \text{ }\mu\text{m}$ , length =  $3 \text{ mm}$ ) were kindly supplied by Schawrzalder Textil-Werke Heinrich Kautzmann (Schenkenzell, GmbH). TEMPO (purity  $\geq 98.0\%$ ), sodium bromide (purity  $\geq 99.0\%$ ), sodium chloride (purity  $\geq 99.0\%$ ) and sodium borohydride (purity  $\geq 98.0\%$ ) were purchased from Sigma Aldrich (Dorset, UK). Sodium hydroxide (Alfa Aesar, 0.5 N), sodium hypochlorite solution (GPR RECTAPUR<sup>®</sup>, 12%  $\text{Cl}_2$  in aqueous solution), hydrochloric acid (AVS TITRINORM<sup>®</sup>, 0.1 N), acetone (GPR RECTAPUR<sup>®</sup>, purity  $\geq 99.5\%$ ), 1,4-dioxane (GPR RECTAPUR<sup>®</sup>, purity  $\geq 99.0\%$ , stabilised with 25 ppm ionol), dimethyl sulfoxide (GPR RECTAPUR<sup>®</sup>, purity  $\geq 99.0\%$ ), formamide (TECHNICAL, purity  $\geq 99.7\%$ ) and ethylene glycol (Reag. Ph. Eur., purity  $\geq 99.0\%$ ) were purchased from VWR International Ltd. (Lutterworth, UK). All chemicals were used as received without further purification.

### TEMPO-mediated oxidation of cellulose

The TEMPO-mediated oxidation of cellulose was conducted following a previously described protocol (Saito and Isogai 2004). Briefly, 10 g of pressed

dissolving pulp sheet was cut into 10 mm × 10 mm pieces and soaked in 1 L of deionized water for 24 h. The mixture was then blended at 40,000 rpm for 3 min using a kitchen blender (Optimum 9400, Froothie Ltd., Cranleigh, UK) to produce a homogenous dissolving pulp suspension (0.1 wt%). To this suspension, TEMPO (0.16 g, 0.1 mmol) and sodium bromide (1.0 g, 1.0 mmol) were added and magnetically stirred. Once the added TEMPO and sodium bromide have fully dissolved, 65 mL of 12% Cl<sub>2</sub> aqueous sodium hypochlorite solution (corresponding to 10 mmol of NaClO per gram of cellulose) was pipetted into this suspension to start the cellulose oxidation reaction. The pH of the suspension was monitored (HI-2550, Hanna Instruments, UK) and maintained at a value of 10 through the titration of 0.5 N sodium hydroxide. The cellulose oxidation reaction was conducted for 5 h at room temperature. The reaction medium was then quenched with 100 mL of deionized water and the TEMPO-oxidised cellulose (TOC) was recovered through centrifugation (SIGMA 4-16S, SciQuip Ltd., UK, 3000 rpm, 3 min). It was then repeatedly washed with 1.5 L of deionised water and centrifuged until the resulting TOC suspension reached a neutral pH. The prepared TOC was then reduced with sodium borohydride following an earlier work (Takaichi et al. 2014). This step was carried out to convert the C6-aldehydes and C2/3-ketones into hydroxyl groups to increase the thermal stability and reduce heat-induced discoloration of TOC as elevated temperature was used in subsequent composite processing. The reduction reaction was carried out for 3 h at room temperature under magnetic stirring at a TOC consistency of 0.1 wt.-% and a sodium borohydride-to-TOC mass ratio of 0.1 g of sodium borohydride per gram of TOC. After the reaction, the TOC was purified following the previously described washing-centrifugation step. The resulting sodium borohydride-reduced *micrometre-sized* TEMPO-oxidised cellulose fibres (TOCF) are herein termed TOCF-Na as the TOC contains sodium counterions. The sample was stored in its never-dried state at 2 wt% solid content in a 4 °C fridge prior to subsequent use.

#### Ion exchange treatment of TOCF-Na

An ion exchange treatment was also carried out on TOCF-Na to convert the sodium carboxylate groups to free carboxyl groups. This ion exchange treatment was

performed at a TOCF-Na consistency of 0.1 wt%. To this suspension, 0.1 N hydrochloric acid was added until the suspension reached a pH of 4. The suspension was then left to stir for 1 h at room temperature. After the ion exchange treatment, the sample was purified following the previously described washing-centrifugation step until a neutral pH was attained. The resulting TOCF containing free carboxyl groups are herein termed TOCF-H. The sample was also stored in its never-dried state at 2 wt% solid content in a 4 °C fridge prior to subsequent use.

#### Preparation of TOCN

The previously prepared TOCF-Na was subjected to mechanical disintegration to produce TOCN. The mechanical disintegration process was carried out at a consistency of 0.1 wt% in batches of 500 mL using a blender (Optimum 9400, Froothie Ltd., Cranleigh, UK) operating at 40,000 rpm for 3 min. The TOCN suspension was stored at a consistency of 0.1 wt% in a 4 °C fridge prior to subsequent use.

#### Processing of (TEMPO-oxidised) cellulose-reinforced polypropylene (PP) composites

Majority of the TOCN-reinforced polymer composite fabrication methods reported in the literature are based on solution casting, whereby TOCN is first dispersed in a polymer solution, followed by solvent evaporation (Johnson et al. 2009; Fujisawa et al. 2012; Bulota et al. 2013; Wang et al. 2018) and an optional compression moulding step (Wang et al. 2015; Noguchi et al. 2020). Melt compounding of TOCN-reinforced thermoplastic starch based on liquid feeding has also been reported (Hietala et al. 2014). In this work, PP composites reinforced with 5 wt% (TEMPO-oxidised) cellulose were fabricated using polymer melt extrusion but based on a dry feeding process. Prior to melt extrusion, the chopped PP fibres were pre-mixed with (TEMPO-oxidised) cellulose at a mass ratio of 95:5 (dry basis) in water at a consistency of 0.1 wt% (relative to cellulose) using an overhead stirrer (Hei-Torque 100, Heidolph Instruments GmbH & Co. KG, 6 mm diameter three-blade impeller, 300 rpm) for 3 min. The wet pre-mix was then freeze dried (Alpha 1-2 LDplus, Martin Christ, Osterode, Germany) to produce dry (TEMPO-oxidised) cellulose-PP pre-mix prior to feeding it into a co-rotating twin-screw

extruder (Eurolab XL, screw diameter = 16 mm, L/D = 25, Thermofischer Scientific, Karlsruhe, Germany). Melt extrusion was performed at 175 °C with a screw speed of 300 rpm and a throughput of  $2.3 \pm 0.1 \text{ kg h}^{-1}$ . The extrudate was then pelletised (VariCut Thermofischer Scientific, Karlsruhe, Germany) and injection moulded (Haake Minijet Pro, Thermofischer Scientific, Karlsruhe, Germany) into dog bone and rectangular shaped test specimens. The barrel and mould temperatures of the injection moulder were kept at 185 °C and 40 °C, respectively. The sample was injection moulded at an injection pressure and time of 650 bar and 30 s, respectively, followed by a post-pressure of 650 bar for a further 90 s. The injection moulded tensile dog bone test specimens had an overall length of 65 mm, a gauge length of 10 mm, a thickness of 3 mm and the narrowest part of the dog bone specimen was also 3 mm. The injection moulded rectangular test specimens, used in subsequent single-edge notched fracture toughness test and dynamic mechanical thermal analysis, had an overall length of 80 mm, a width of 13 mm and a thickness of 3 mm.

Characterisation of (TEMPO-oxidised) cellulose and their respective PP composites

#### *Carboxylate content of dissolving pulp and TEMPO-oxidised cellulose*

The carboxylate content of dissolving pulp and TOC was determined using conductometric titration method reported by Araki et al. (2001). Briefly, the sample (0.1 g, dry basis) was dispersed in 55 mL of deionised water and 5 mL of 10 mM NaCl solution was then added to this suspension. The pH of this suspension was adjusted to 3 through the titration of 0.1 N HCl. A 40 mM NaOH solution was added dropwise at a rate of  $0.1 \text{ mL min}^{-1}$  until the pH of the suspension reached 11. The conductivity of the suspension between the pH of 3 and 11 was recorded (HI-2550, Hanna Instruments, UK) and the carboxylate content of the (TEMPO-oxidised) cellulose was then calculated based on the conductivity of the weak acid groups.

#### *Morphology of dissolving pulp and TEMPO-oxidised cellulose*

The morphology of dissolving pulp, TOCF-Na and TOCF-H was investigated using a large chamber scanning electron microscopy (SEM) (S-3700N, Hitachi, Tokyo, Japan). An accelerating voltage of 15 kV was used. The samples were mounted onto aluminium stubs and Au coated (Automatic sputter coater, Agar Scientific, Stansted, UK) using a coating current of 40 mA for 20 s prior to SEM. To characterise the morphology of TOCN, transmission electron microscopy (TEM) was used. Briefly, 3  $\mu\text{L}$  of 0.0125 wt% TOCN suspension was deposited onto a PELCO<sup>®</sup> TEM 300 mesh copper grid with ultrathin carbon support film (CF300-Cu-UL, obtained from Ted Pella, Inc., hydrophilized by an Emitech K100X glow discharge – Carbon glow discharge unit). After 2 min, the water droplet was carefully removed by blot drying using the sharp edge of a cut filter paper (Whatman<sup>®</sup> qualitative filter paper, Grade 2). To improve contrast, the TOCN was stained with 2 wt% aqueous solution of uranyl acetate by placing the coated sample-bearing side of the grid on a drop of the staining solution. The extra staining solution was blot dried using filter paper after 60 s and washed one time by repeating this procedure using a water drop. After the blot drying step, the sample was left for 5 min to completely dry at ambient temperature. TEM imaging was conducted using a JEOL 2800 analytical high resolution TEM. Single tilt sample manipulation was used. The voltage and current used were 200 kV and 155  $\mu\text{A}$ , respectively.

#### *Critical surface tension ( $\gamma_c$ ) of dissolving pulp and TEMPO-oxidised cellulose*

The  $\gamma_c$  of dissolving pulp and TOC was determined using capillary rise technique (Krüss K100 Tensiometer, software version K3.1, Hamburg, Germany) based on the wicking of test liquids with different surface tensions ( $\gamma_{LV}$ ) (Tröger et al. 1998). Freeze-dried sample (0.1 g) was packed into a cylindrical container with a height of 46 mm and a diameter of 12 mm. The bottom of this sample container consisted of 20 small holes which allowed for the wicking of the test liquid into the sample. Prior to the measurement, the sample container was mounted onto the ultra-sensitive microbalance (resolution of 0.01 mg) of the

instrument. The reservoir containing the test liquid was then moved upwards. Upon contact with the sample container, the movement of the test liquid reservoir was stopped immediately to ensure that the mass gained detected by the instrument was a result of only capillarity. The mass gain of the sample was recorded as a function of time and the obtained data was analysed using the Washburn equation for single capillary (Szekely et al. 1971):

$$\gamma_{LV} \cos \theta = \left[ \frac{2}{A^2 r} \right] \left[ \frac{\eta}{\rho^2} \right] \left[ \frac{\Delta m^2}{t} \right] \quad (1)$$

whereby  $\gamma_{LV}$ ,  $\eta$  and  $\rho$  are the surface tension, viscosity and density of test liquid, respectively. The symbols  $\Delta m$ ,  $A$ ,  $r$ ,  $\theta$  and  $t$  correspond to the initial mass gain of the sample during the test, cross-sectional area of the capillary, radius of the capillary, contact angle and time, respectively. As the geometry of the capillary in the sample was not well-defined, Eq. (1) was further simplified by assuming  $\frac{A^2 r}{2} = C$ , i.e. the geometry of the capillary is constant throughout the measurement (Grundke et al. 1996), resulting in:

$$C \gamma_{LV} \cos \theta = \left[ \frac{\eta}{\rho^2} \right] \left[ \frac{m^2}{t} \right] \quad (2)$$

By plotting the normalised initial wetting rates as a function of test liquid surface tension,  $\left[ \frac{\eta}{\rho^2} \right] \left[ \frac{m^2}{t} \right] = f(\gamma_{LV})$ , the  $\gamma_c$  of the sample can be determined from the maxima of the plot.

#### *Thermal degradation behaviour of (TEMPO-oxidised) cellulose-reinforced PP composites*

The thermal degradation behaviour of dissolving pulp, TOC, as well as their respective (TEMPO-oxidised) cellulose-reinforced PP composites was investigated using thermal gravimetric analysis (Discovery TGA, TA Instruments, Elstree, UK). Approximate 5 mg of sample was heated from room temperature to 500 °C at a rate of 10 °C min<sup>-1</sup> in a N<sub>2</sub> atmosphere (50 mL min<sup>-1</sup>).

#### *Differential scanning calorimetry (DSC) of (TEMPO-oxidised) cellulose-reinforced PP composites*

The crystallisation and melting behaviour of (TEMPO-oxidised) cellulose-reinforced PP

composites were investigated using DSC (Discovery DSC, TA Instruments, Elstree, UK) in N<sub>2</sub> atmosphere. A heat-cool-heat regime was employed. Approximate 8 mg of sample was heated from room temperature to 200 °C at a rate of 10 °C min<sup>-1</sup> before cooling to room temperature at a rate of 50 °C min<sup>-1</sup>. The sample was then re-heated to 200 °C at the same rate of 10 °C min<sup>-1</sup>. The crystallinity ( $\chi_c$ ) of the PP composites was calculated from:

$$\chi_c(\%) = \frac{\Delta H_m}{(1 - w_f) \Delta H_m^o} \times 100 \quad (3)$$

where  $w_f$  is the weight fraction of the (TEMPO-oxidised) cellulose in the PP composite,  $\Delta H_m$  is the melting enthalpy evaluated from the DSC curve and  $\Delta H_m^o$  is the melting enthalpy of crystalline PP (207 J g<sup>-1</sup>) (Gee and Melia 1970).

#### *Tensile properties of (TEMPO-oxidised) cellulose-reinforced PP composites*

Tensile test was conducted in accordance with ASTM D638-14 using a universal testing machine (Model 4502, Instron, High Wycombe, UK) equipped with a 10 kN load cell. A crosshead displacement speed of 10 mm min<sup>-1</sup> was used. Prior to the test, two dots were marked on the surface of each dog bone test specimen in the direction of applied load. The strain of the test specimen was then evaluated by monitoring the movement of these two dots using a non-contact optical extensometer (iMetrum Ltd., Bristol, UK). An average of 5 specimens were tested for each sample.

#### *X-ray micro-computed tomography ( $\mu$ CT) of TEMPO-oxidised cellulose-reinforced PP composites*

To investigate the dispersion of dissolving pulp and the various TEMPO-oxidised cellulose samples in the PP matrix, X-ray  $\mu$ CT was performed using a Zeiss Xradia 520 Versa 3D X-ray microscope (Carl Zeiss AG, Germany) operating at a voltage of 40 kV and a power of 3 W. A sample measuring 30 × 120 mm was cut from the injection moulded rectangular test specimen and used in this characterisation.  $\mu$ CT images with a voxel size of 3.5  $\mu$ m and a field of view diameter of 3 mm were acquired using a 0.4 × optical objective. The reconstruction and



segmentation of the  $\mu$ CT images were performed using 3D Slicer 4.11.

#### *Single-edge notched fracture toughness of (TEMPO-oxidised) cellulose-reinforced PP composites*

The fracture toughness of neat PP and (TEMPO-oxidised) cellulose-reinforced PP composites was determined from single edge-notch beam (SENB) specimens. The test was conducted in accordance with ASTM D 5045-14. Prior to the test, a notch with a depth 5.5 mm was introduced at the half way point lengthwise in the width direction of the SENB test specimen using a band saw (Startrite 502S, A.L.T. Saws & Spares Ltd., Kent, UK). The notch was further sharpened by tapping a sharp scalpel at the tip of the notch. The initial crack length ( $a$ ) to width ( $w$ ) ratio,  $x$ , of the SENB test specimen was 0.47. The SENB test specimen was then loaded in three-point bending mode at a crosshead displacement speed of 10 mm min<sup>-1</sup> using a universal tester (Model 4502, Instron, High Wycombe, UK) equipped with a 10 kN load cell. The span length used was 50 mm. An average of 4 specimens were tested for each type of sample. The initial stress intensity factor,  $K_{IC}$ , of the SENB test specimen was calculated using

$$K_{IC} = \left( \frac{P}{bw^{0.5}} \right) \times f(x) \quad (4)$$

where  $P$  is the load at crack initiation,  $b$  is the thickness of the sample and  $f(x)$  is:

$$f(x) = 6\sqrt{x} \times \left( \frac{1.99 - x(1-x)(2.15 - 3.93x + 2.7x^2)}{(1+2x)(1-x)^{1.5}} \right) \quad (5)$$

#### *Fracture morphology of (TEMPO-oxidised) cellulose-reinforced PP composites*

The SENB fracture surface of the model PP composites was investigated using SEM (S-3700N, Hitachi, Tokyo, Japan) following the previously described protocol. The SENB fractured samples were mounted upright onto aluminium stubs such that the fracture plane can be observed. The samples were Au coated (Automatic sputter coater, Agar Scientific, Stansted,

UK) using a coating current of 40 mA for 20 s prior to SEM. The accelerating voltage used was 15 kV.

#### *Viscoelastic properties of (TEMPO-oxidised) cellulose-reinforced PP composites*

The viscoelastic properties of neat PP and model PP composites were characterised using dynamic mechanical thermal analysis (DMTA) (RSA G-2 Solids Analyzer, TA Instruments, Elstree, UK). DMTA was performed in three-point bending mode with a span length of 40 mm. The storage and loss moduli, as well as the energy dissipation factor ( $\tan \delta$ ) were measured from  $-50$  to  $150$  °C using a heating rate of  $5$  °C min<sup>-1</sup>, a strain amplitude of 0.1% and frequency of 1 Hz.

## Results and discussion

### Carboxylate content and morphology of various (TEMPO-oxidised) cellulose

Table 1 summarises the carboxylate contents of dissolving pulp and the various TOC prepared in this work. The carboxylate content increased from 0.06 mmol/g for dissolving pulp to 1.5 mmol/g for TOC. No differences were observed in the carboxylate content of TOCF-Na, TOCF-H and TOCN, as all the samples were prepared under the same oxidation condition. Figure 1 shows the visual appearance of the various (TEMPO-oxidised) cellulose in water suspensions at 0.1 wt% consistency. Clear sedimentation at the bottom of the vial can be observed for the dissolving pulp suspension. However, both the TOCF-Na and TOCF-H suspensions remained stable with no observable sedimentation even after 48 h. This is due to the introduction of anionically-charged moieties onto the surface of these TOC samples, which increases the thickness of the electrochemical double layer. Streaming potential measurements showed that TOC possessed a  $\zeta$ -potential plateau of ca.  $-40$  mV whilst the  $\zeta$ -potential plateau of neat and unmodified cellulose was only  $-10$  mV (both measured in 1 mM KCl supporting electrolyte) (Mautner et al. 2014, 2015). The high magnitude of  $\zeta$ -potential plateau led to the formation of a stable TOC-in-water suspension.

**Table 1** The carboxylate content, critical surface tension ( $\gamma_c$ ) and onset thermal degradation ( $T_{d,onset}$ ) of dissolving pulp and the various TOC samples prepared

Sample	Carboxylate content (mmol/g)	$\gamma_c$ (mN m <sup>-1</sup> )	$T_{d,onset}$ (°C)
Dissolving pulp	0.06 ± 0.02	45.5 ± 1.0	271
TOCF-Na	1.51 ± 0.19	42.5 ± 0.2	236
TOCF-H	1.51 ± 0.15	43.8 ± 1.5	238
TOCN	1.53 ± 0.10	42.9 ± 2.5	227

The translucency of the TOCF-Na and TOCF-H suspensions can be attributed to the presence of large TOC fibres. Without mechanical disintegration, the width of both TOCF-Na and TOCF-H was found to be  $\sim 17 \mu\text{m}$  (see fibre width distribution on Fig. 1, right column), similar to that of dissolving pulp fibres despite their high carboxylate content. However, the presence of surface microfibrillation (see arrow in Fig. 1, middle column) on TOCF-Na and TOCF-H can be observed, which is due to the onset of cellulose fibril individualisation. By comparison, TOCN suspension was transparent, consistent with the observation by Saito et al. (2007) for TOCN at similar carboxylate content. This also indicates the successful individualisation of the micrometre-sized TOCF-Na ( $\sim 17 \mu\text{m}$  in fibre width) to nano-sized TOCN with a fibre width of  $\sim 9 \text{ nm}$ .

#### Wetting behaviour and $\gamma_c$ of various (TEMPO-oxidised) cellulose

The wetting behaviour of (TEMPO-oxidised) cellulose was quantified in this work to delineate any improvements in the mechanical properties of the resulting model PP composites from their surface chemistry. The  $\gamma_c$  of a solid, defined as the surface tension at which an imaginary liquid just completely wets the surface (Zisman 1964), was determined from the wicking of various test liquids into a packed bed of (TEMPO-oxidised) cellulose. A typical wetting curve, i.e.  $\Delta m^2 = f(t)$ , is shown in Fig. 2a. The initial slope of the wetting curve corresponds to the wicking of the test liquid into the sample due to capillarity. This is then followed by a plateau, which is caused by an equilibrium between capillary and gravitational forces (Tröger et al. 1998). By plotting the normalised wetting rate (right hand side of Eq. 2) based on the

initial slope of the wetting curve as a function of the surface tension of the various test liquids,  $\gamma_c$  of the sample can be determined from the maxima of this plot (Fig. 2b). The data in Fig. 2b were fitted with a Gaussian curve. This maxima is analogous to the Zisman's critical solid-vapor surface tension (Tröger et al. 1998). Liquids with surface tension lower than  $\gamma_c$  (i.e. the maxima of the plot) will fully wet the sample whilst only partial wetting of the sample can be achieved with liquids with surface tension higher than  $\gamma_c$ .

The  $\gamma_c$  of the (TEMPO-oxidised) cellulose are summarised in Table 1. Dissolving pulp was found to possess a  $\gamma_c$  of  $45.5 \text{ mN m}^{-1}$  and this agrees well with the  $\gamma_c$  reported by Luner and Sandell (1969) for regenerated cellulose film derived from cotton, which is also pure cellulose without the presence of hemicellulose. It can also be seen from Table 1 that all TOC samples were found to possess similar  $\gamma_c$ , independent of the fibre width of the TOC, indicating that the TEMPO-mediated oxidation reaction does not alter the surface energetics of cellulose. This could be attributed to the fact that substituting the C6 hydroxyl groups with carboxyl groups does not significantly affect the polar component of the surface energy of cellulose (Sacui et al. 2014). Henceforth, any improvements observed in the measured mechanical properties of the resulting (TEMPO-oxidised) cellulose-reinforced PP composites would not be a direct result of any improvements in the cellulose (nano)fibre-matrix interface due to the introduction of carboxylate/carboxyl groups.

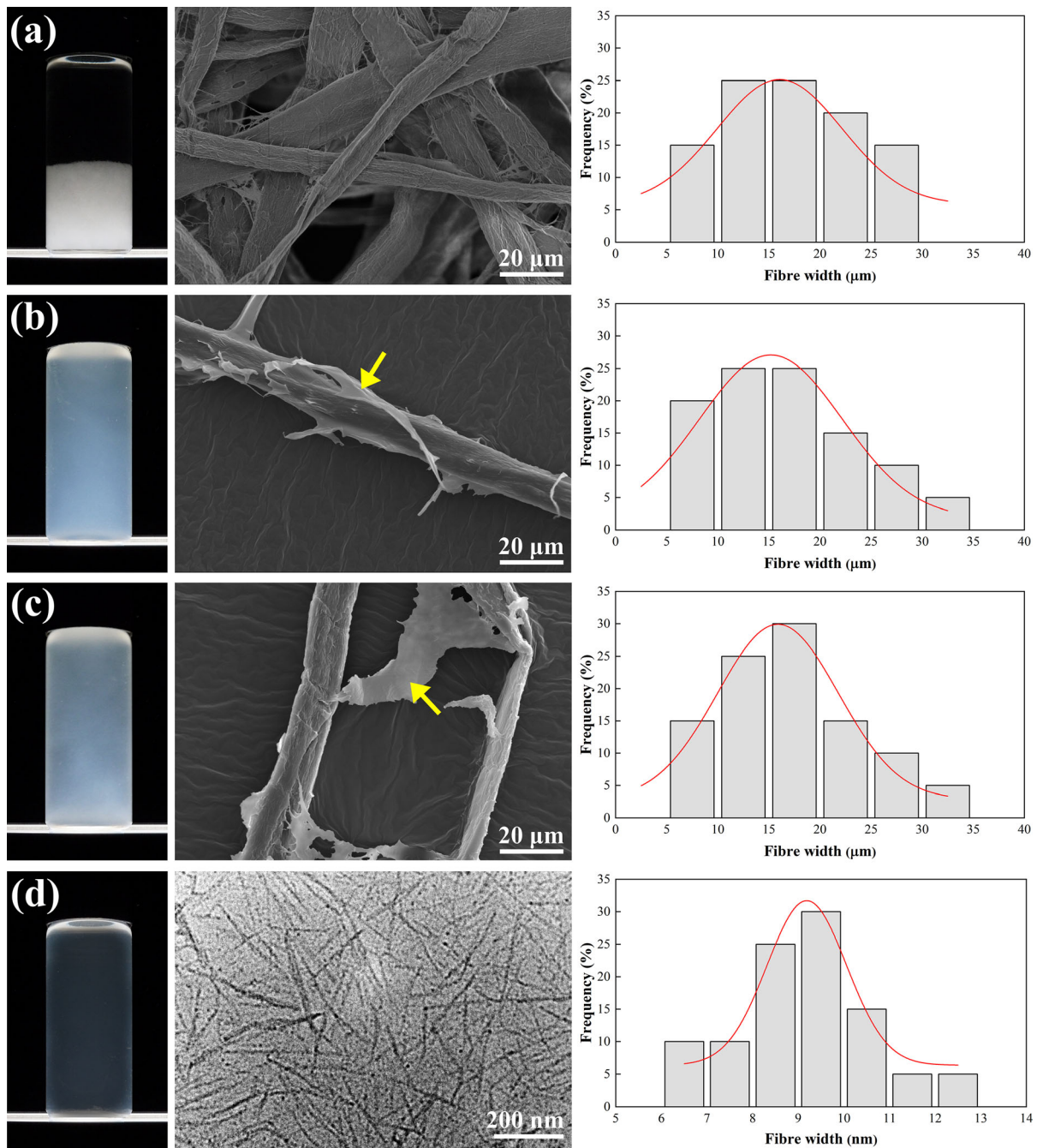


**Fig. 1** Dispersion state of cellulose suspension at 0.1 wt% consistency after 48 h (left column), morphology of the (TEMPO-oxidised) cellulose (middle column) and fibre width

distribution (right column) of **a** dissolving pulp, **b** TOCF-Na, **c** TOCF-H and **d** TOCN. The yellow arrows show the presence of surface microfibrillation on TOCF-Na and TOCF-H



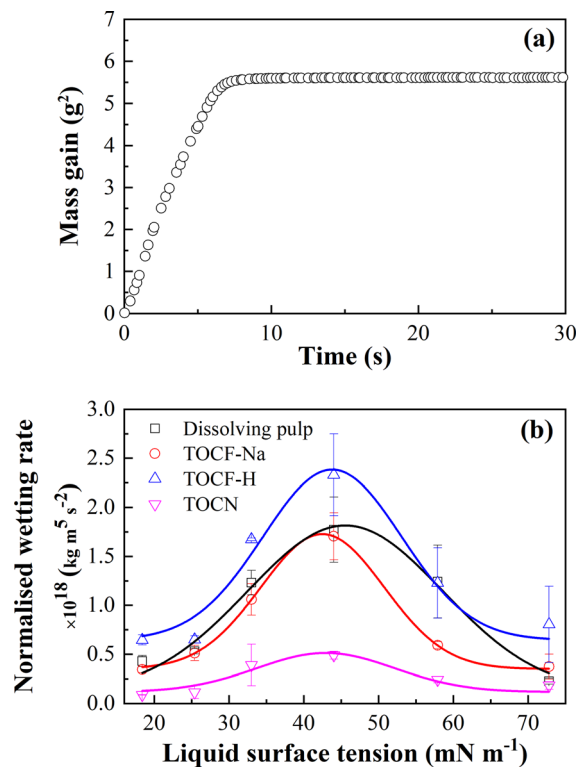


**Fig. 2** Wetting behaviour of dissolving pulp and the various TOC samples. **a** Exemplar wetting curve of dissolving pulp using water as the test liquid. **b** Normalised wetting rates of dissolving pulp and the various TOC samples as a function of liquid surface tension

Thermal degradation behaviour of various (TEMPO-oxidised) cellulose and their respective model PP composites

The thermal degradation behaviour of dissolving pulp, TOCF-Na, TOCF-H and TOCN in  $N_2$  atmosphere are shown in Fig. 3a. Their respective onset thermal degradation temperatures ( $T_{d,onset}$ ) are tabulated in Table 1. It can be seen from Fig. 3a that all samples underwent multiple thermal degradation steps. The initial thermal decomposition of dissolving pulp between 300 and 350 °C can be attributed to the cleavage of the glycosidic linkages of cellulose (Dietenberger and Hasburgh 2016; Santmartí and Lee 2018). During this degradation step, two reactions occurred: (i) the partial cross-linking of cellulose molecules, resulting in the formation of char and (ii) the depolymerisation of the cellulose chains, converting cellulose into tar (Mamleev et al. 2007). The initial thermal degradation of the TOC samples occurring

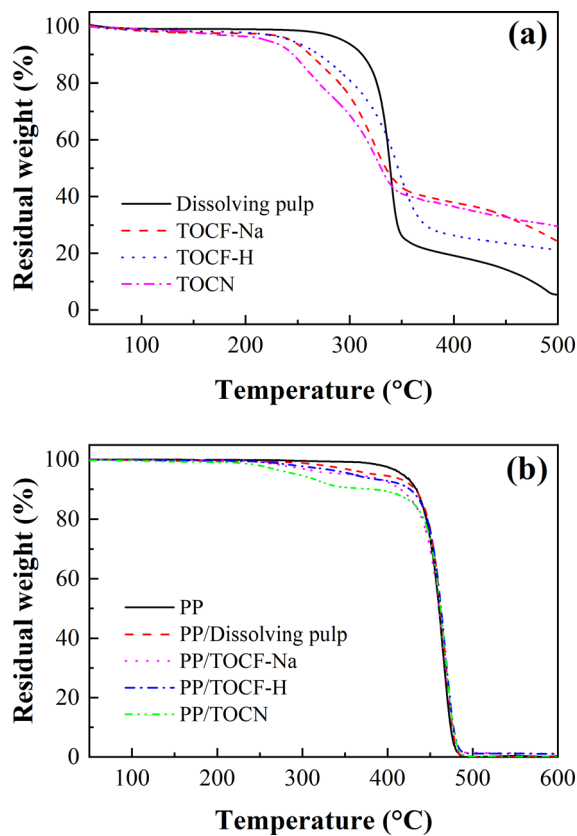


**Fig. 3** Thermal degradation behaviour of **a** (TEMPO-oxidised) cellulose and **b** (TEMPO-oxidised) cellulose-reinforced PP composites

between 150 and 250 °C can be attributed to the decarboxylation of TOC (Fukuzumi et al. 2010; Lichtenstein and Lavoine 2017). This is then followed by the cleavage of glycosidic linkages of cellulose at 300–350 °C. It can also be observed from Fig. 3a that TOCF-H exhibited slower thermal degradation rate compared to TOCF-Na. This is because the rate of thermal degradation of the TOCF is governed by the decarboxylation of the thermally unstable sodium anhydroglucuronate unit, which is present in TOCF-Na (Fukuzumi et al. 2009; Lichtenstein and Lavoine 2017). However, the  $T_{d,onset}$  of TOCF-Na and TOCF-H were found to be similar (see Table 1), indicating that the structural difference between the sodium carboxylate groups in TOCF-Na and the free carboxyl groups in TOCF-H had little influence on  $T_{d,onset}$ .

TOCN was found to possess the lowest  $T_{d,onset}$  and degrade at a much faster rate than TOCF-Na. This is rather surprising as TOCN and TOCF-Na are

essentially the same TOC chemically; both samples contain the thermally unstable sodium anhydroglucuronate. Since TOCN and TOCF-Na possessed the same carboxylate content, this difference in the thermal degradation behaviour must be due to the difference in the fibre width between TOCN and TOCF-Na. The smaller fibre width and hence, the higher exposed area of TOCN could accelerate its rate of thermal degradation compared to TOCF-Na, which possessed a larger fibre width. Increased reactivity due to increased accessibility is a well-recognized fact in liquid/solid systems upon cellulose modification (Ye and Farriol 2005). Figure 3b shows the thermal degradation behaviour of neat PP and model PP composites reinforced with (TEMPO-oxidised) cellulose. PP underwent single thermal degradation step whilst a two-step thermal degradation process was observed for (TEMPO-oxidised) cellulose-reinforced PP composites, with a lower  $T_{d,onset}$  (Table 2). This is consistent with the lower thermal stability of the (TEMPO-oxidised) cellulose reinforcement.

#### Crystallisation and melt behaviour of neat PP and its model (TEMPO-oxidised) cellulose-reinforced PP composites

Trans-crystallisation of PP is known to occur from the surface of cellulose fibres (Gray 2008). This could lead to a significant increase in the crystallinity of the PP matrix in the various model composites prepared. Consequently, this would complicate the delineation of the effects of PP crystallinity and the reinforcing ability of TOC of different fibre widths when

analysing the mechanical properties of the model composites. Therefore, DSC was conducted to investigate the crystallisation and melt behaviour of PP and the various model PP composites prepared (Fig. 4). Their characteristic crystallisation and melting temperatures are tabulated in Table 2, along with the degree of crystallinity of the PP matrix. A single melting peak at  $\sim 166$  °C and a single crystallisation peak at  $\sim 106$  °C were observed. The crystallinity of all the samples was found to be similar at  $\sim 45\%$ , suggesting that cellulose-induced trans-crystallisation of PP did not occur in the composite samples. This could be due to the low loading fraction of (TEMPO-oxidised) cellulose in the PP composites. Nevertheless, the similarity in the crystallinity of neat PP and PP composites reinforced with (TEMPO-oxidised) cellulose of different fibre widths calculated based on the 1st heating DSC thermograms implies that a direct comparison in the mechanical properties of the samples can be made. It is also worth mentioning that the  $T_g$  of PP was not detected by DSC as this transition is typically weak. Therefore, DMTA was used to detect the  $T_g$  of PP (see the viscoelastic behaviour of model PP composites section). The 2nd heating DSC thermograms also showed the presence of double melting peaks. This can be attributed to the transition between different modifications of the alpha crystal form due to the fast cooling rate employed in our DSC measurement ( $50$  °C  $\text{min}^{-1}$ ), which may have promoted primary and secondary crystallisations (Paukeri and Lehtinen 1993).

**Table 2** The thermal properties of (TEMPO-oxidised) cellulose-reinforced PP composites.  $T_{d,onset}$ ,  $T_m$ ,  $\chi_c$  and  $T_c$  correspond to the onset thermal degradation temperature determined

from TGA, as well as melting temperature, crystallinity and crystallisation temperature determined from DSC, respectively

Sample	$T_{d,onset}$ (°C)	First heating		Cooling $T_c$ (°C)	Second heating	
		$T_m$ (°C)	$\chi_c$ (%)		$T_m$ (°C)	$\chi_c$ (%)
PP	356	166	42	105	164	43
PP/Dissolving pulp	265	165	45	105	165	46
PP/TOCF-Na	246	166	44	107	164	45
PP/TOCF-H	255	165	43	108	163	46
PP/TOCN	220	166	43	108	164	44

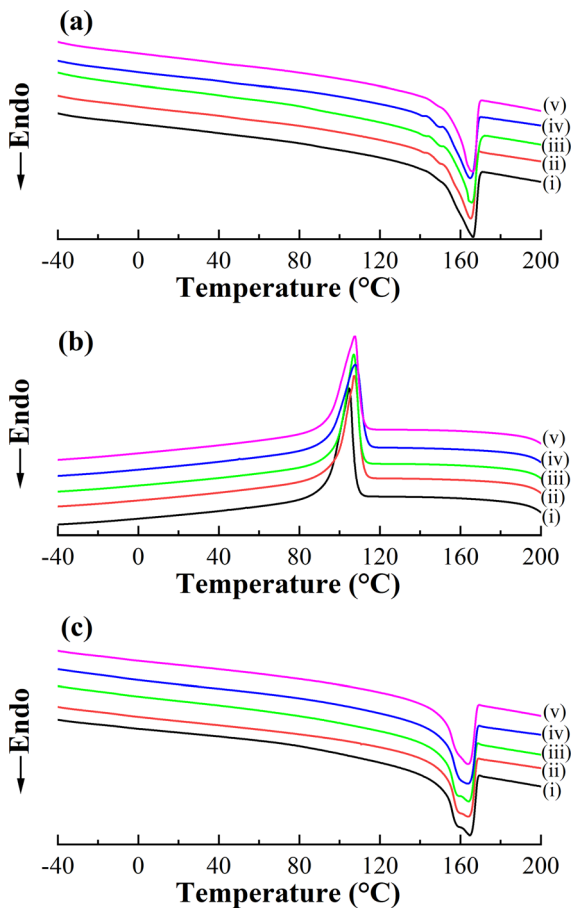


**Fig. 4** DSC thermograms of neat PP and its (TEMPO-oxidised) cellulose-reinforced PP composites based on **a** first heating, **b** cooling and **c** second heating. Samples (i)–(v) denote neat PP, PP/dissolving pulp, PP/TOCF-Na, PP/TOCF-H and PP/TOCN, respectively

### Tensile properties of model (TEMPO-oxidised) cellulose-reinforced PP composites

Table 3 summarises the tensile properties of neat PP and model (TEMPO-oxidised) cellulose-reinforced PP composites. The tensile modulus of PP was measured to be 1.8 GPa and the introduction of only 5 wt% dissolving pulp as reinforcement increased the tensile modulus to 2.2 GPa. When PP was reinforced with 5 wt% of TOCF-Na and TOCF-H, a tensile modulus of up to 2.5 GPa was achieved. This represents a  $\sim 36\%$  increase over neat PP. As the crystallinity of neat PP and model (TEMPO-oxidised) cellulose-reinforced PP composites was found to be similar (Table 2), the observed improvements must be due to the introduction of (TEMPO-oxidised) cellulose as reinforcement. Since dissolving pulp and the various TOC samples possessed similar  $\gamma_c$  (Table 1), the observed higher tensile modulus of PP/TOCF-Na and PP/TOCF-H compared to PP/dissolving pulp and PP/TOCN can be attributed to the differences in fibre morphology. We postulate that the presence of surface microfibrillation on TOCF-Na and TOCF-H (see Fig. 1, middle column, yellow arrows) led to improved mechanical interlocking and the local stiffening of the PP matrix around TOCF-Na/H, improving the quality of the fibre-matrix interface. Similar effects have been observed in hierarchically structured composites reinforced with micrometre-sized sisal fibres coated with nano-sized bacterial cellulose (Lee et al. 2012). X-ray  $\mu$ CT images (Fig. 5) also showed that TOCN is highly agglomerated in the

**Table 3** The mechanical and viscoelastic properties of PP and its (TEMPO-oxidised) cellulose-reinforced PP composites

Sample	$E$ (GPa)	$\sigma$ (MPa)	$K_{IC}$ (MPa m <sup>1/2</sup> )	$E'$ at 20 °C (GPa)	$T_g$ (°C)
Neat PP	1.8 ± 0.2	36.1 ± 1.2	2.87 ± 0.08	1.68 ± 0.09	3.7 ± 0.6
PP/Dissolving pulp	2.1 ± 0.2	36.0 ± 1.7	2.73 ± 0.05	1.98 ± 0.07 <sup>a</sup>	7.2 ± 1.5
PP/TOCF-Na	2.5 ± 0.2 <sup>a</sup>	36.1 ± 0.9	2.95 ± 0.04	2.28 ± 0.08 <sup>a</sup>	7.9 ± 2.0
PP/TOCF-H	2.4 ± 0.1 <sup>a</sup>	35.9 ± 0.9	2.97 ± 0.02	2.27 ± 0.10 <sup>a</sup>	7.7 ± 1.4
PP/TOCN	2.0 ± 0.2	33.8 ± 0.8 <sup>a</sup>	2.52 ± 0.07 <sup>a</sup>	2.17 ± 0.00 <sup>a</sup>	5.4 ± 0.6

$E$ ,  $\sigma$ ,  $K_{IC}$ ,  $E'$  and  $T_g$  denote the tensile modulus, tensile strength, initial critical stress intensity factor, storage modulus and mechanical glass transition temperature, respectively

<sup>a</sup>Mean value is significantly different from the mean of neat PP at 5% significance level based on ANOVA and Tukey-Kramer pairwise comparison

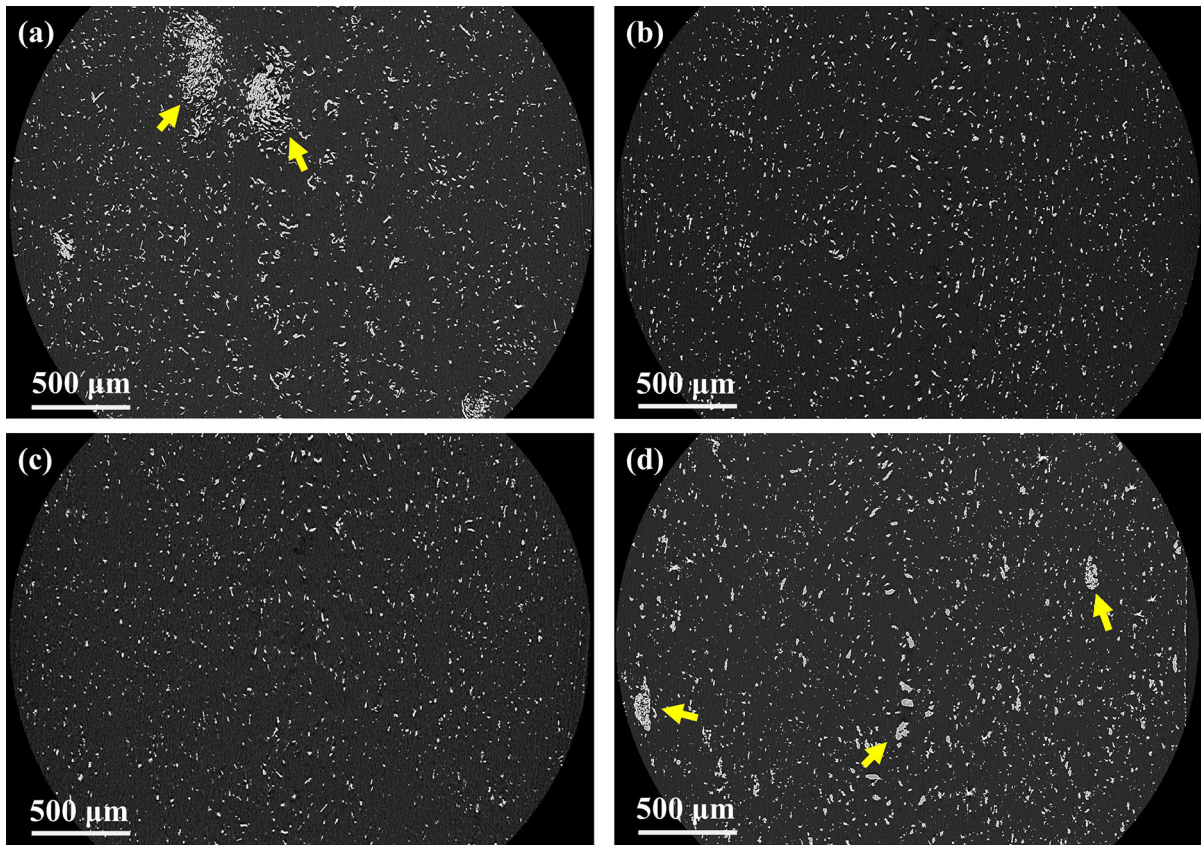


**Fig. 5** X-ray  $\mu$ CT images of PP composites containing 5 wt% **a** dissolving pulp, **b** TOCF-Na, **c** TOCF-H and **d** TOCN. The yellow arrows indicate agglomeration of cellulose (nano)fibres

PP matrix, which further reduced the reinforcing efficiency of TOCN and led to the observed lower tensile modulus of PP/TOCN composite (Geng et al. 2018) compared to PP composites reinforced with TOCFs.

The tensile strength of PP, as well as model PP/dissolving pulp, PP/TOCF-Na and PP/TOCF-H composites was found to be similar at  $\sim 36$  MPa, indicating that the incorporation dissolving pulp and TOCFs did not have any significant influence. The failure of a composite is a complex process, which has not been successfully elucidated for cellulose (nano)-composites (Lee et al. 2014). Nevertheless, the lack of improvements in tensile strength could be due to the small amount (5 wt%) of reinforcement introduced, which is insufficient to impose any obvious improvements. However, there is a noticeable decrease in the tensile strength of PP composite reinforced with TOCN. The model PP/TOCN composite possessed the lowest tensile strength (33.8 MPa); 6% decrease

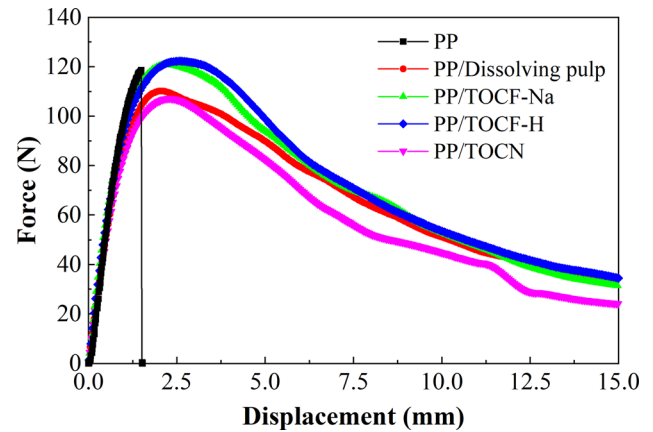
over neat PP and model PP/TOCFs. This can also be attributed to the agglomeration of TOCN in the PP matrix (Fig. 5).

SENB fracture toughness of model (TEMPO-oxidised) cellulose-reinforced PP composites

Figure 6 presents the representative force-displacement curves of PP and model (TEMPO-oxidised) cellulose-reinforced PP composites. The initial slope of the force-displacement curve corresponds to the linear elastic response of the material, followed by yielding and crack propagation. Neat PP failed catastrophically, characterised by a sharp drop in the force-displacement curve once maximum force was reached. Progressive failure, characterised by a continuous and progressive decrease in load after maximum load was reached, was observed for all model (TEMPO-oxidised) cellulose-reinforced PP



**Fig. 6** Representative SENB force-displacement curve of neat PP and its (TEMPO-oxidised) cellulose-reinforced PP composites



composites. To elucidate this further, fractographic analysis was conducted on the fractured SENB test specimens.

The fracture surface of neat PP (Fig. 7a) showed a ‘mirror/mist/hackle’ morphology, which is typical of polymers exhibiting catastrophic failure (Greenhalgh 2009). The ‘mirror’ region observed near the notch region is relatively smooth and linked to slow

propagation as the incipient crack develops. As the fracture accelerates, ‘mist’ region is produced, resulting in a smooth, matt surface in which scarps and riverlines begin to form (see Fig. 7a at 200 × magnification). Further acceleration of the crack to its terminal velocity produced ‘hackle’ morphology consisting of distinct scarps and riverlines. The SENB fracture surface of the model PP composites showed

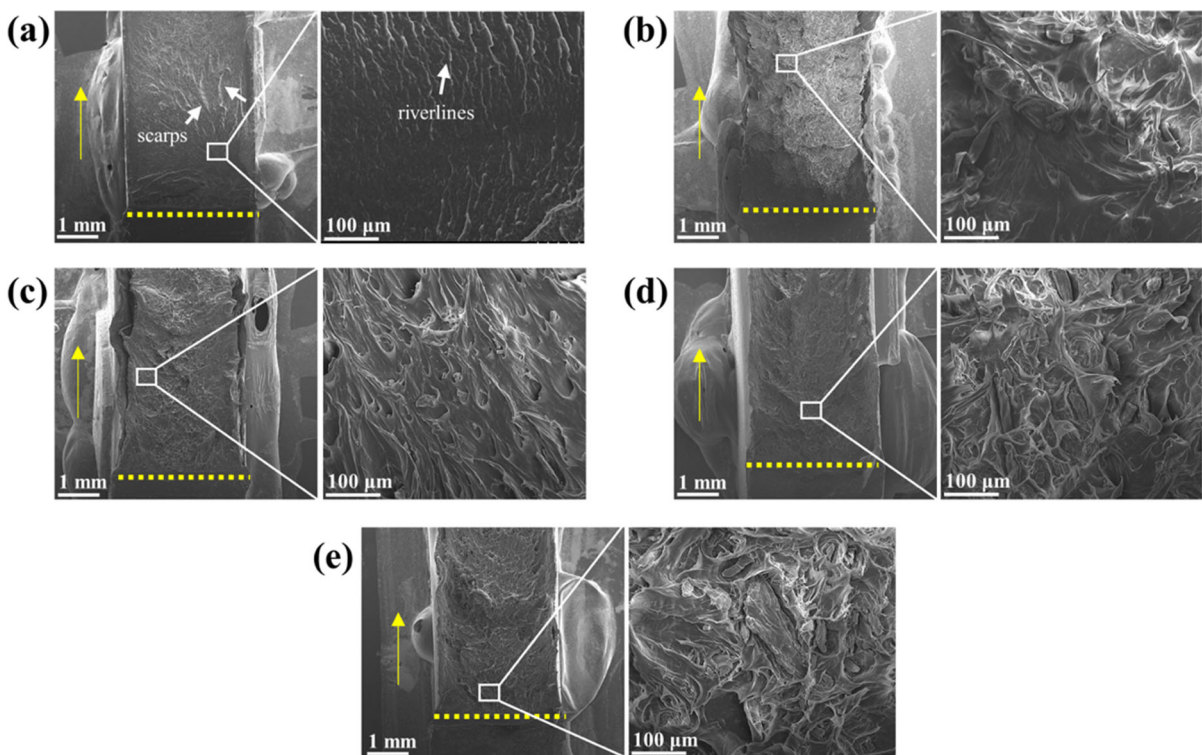


**Fig. 7** Fracture surface of **a** neat PP, **b** PP/dissolving pulp, **c** PP/TOCF-Na, **d** PP/TOCF-H and **e** PP/TOCN SENB specimens. The yellow dotted lines and arrows indicate the notched region where the crack initiated and the direction of crack propagation, respectively



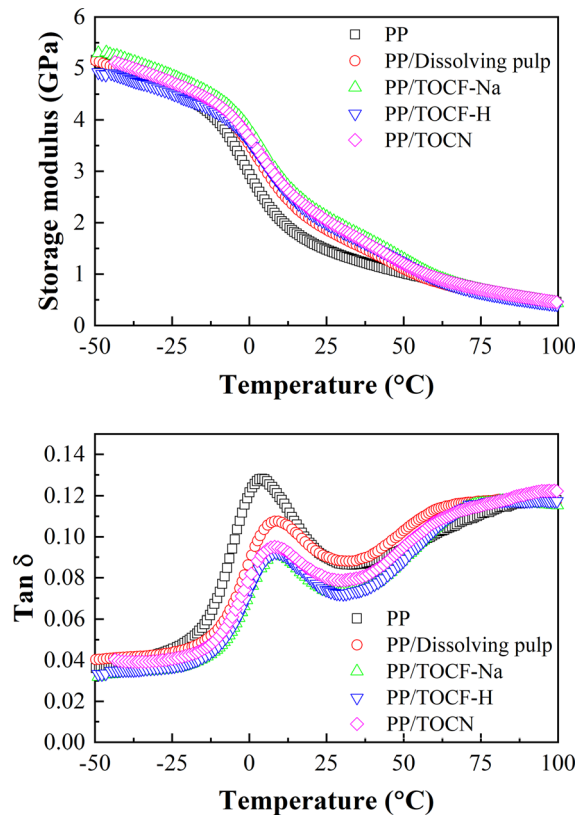
drawing of the PP matrix (Fig. 7b–d). It is hypothesised that during fracture, voids nucleated and developed at the interface between the PP matrix and the reinforcing (TEMPO-oxidised) cellulose. Consequently, the voids grew through plastic deformation until they ultimately coalesce, causing the observed ductile drawing and fibrillation in the SENB fracture surface (Hull 1999). These energy-absorbing mechanisms are responsible for the progressive failure exhibited by the model PP composites.

Table 3 shows the  $K_{IC}$  of neat PP and model PP composites reinforced with (TEMPO-oxidised) cellulose. Neat PP was found to possess a  $K_{IC}$  of 2.87 MPa m<sup>1/2</sup>. The introduction of dissolving pulp fibre as reinforcement led to a 5% decrease in  $K_{IC}$  to 2.73 MPa m<sup>1/2</sup>. A 12% decrease in  $K_{IC}$  value over neat PP to 2.52 MPa m<sup>1/2</sup> was observed when TOCN was used as reinforcement. This is consistent with the low tensile strength of TOCN-reinforced PP composite (see Table 3). However, it is worth mentioning that the  $K_{IC}$  of PP reinforced with TOCF-Na and TOCF-H were found to be  $\sim 2.96$  MPa m<sup>1/2</sup>; a slight improvement over neat PP. This can be attributed to the presence of surface microfibrillation, which increased the energy required to propagate the crack due to improved adhesion through mechanical interlocking and local PP matrix stiffening.

Viscoelastic behaviour of model (TEMPO-oxidised) cellulose-reinforced PP composites

The temperature dependence of the storage modulus ( $E'$ ) and  $\tan \delta$  of neat PP and model PP composites obtained from DMTA are presented in Fig. 8. The respective  $E'$  at 20 °C is summarised in Table 3. It can be seen from this table that  $E'$  of all model (TEMPO-oxidised) cellulose-reinforced PP composites are distinctly higher than that of neat PP. Neat PP possessed a  $E'$  at 20 °C of 1.68 GPa and the model TOCF-Na/H reinforced PP composites possessed  $E'$  at 20 °C of 2.28 GPa;  $\sim 36\%$  improvement over neat PP. However, the model TOCN-reinforced PP composite only showed 29% improvement ( $E' = 2.17$  GPa) over the neat PP. These results corroborated with the tensile modulus of neat PP and model PP composites.

In general, the increase in  $E'$  of the model PP composites is due to the ability of the cellulose reinforcement to restrict the motion of the PP



**Fig. 8** Viscoelastic properties of PP and (TEMPO-oxidised) cellulose-reinforced PP composites

molecular chains (Amash and Zugenmaier 1998; Petersson et al. 2007). As previously discussed, the presence of surface microfibrillation (Fig. 1) on TOCFs led to the local stiffening of the PP matrix. This resulted in higher restriction in the motion of the PP chains and subsequently, higher  $E'$  compared to the model PP/TOCN composite. This is also supported by the shift in mechanical  $T_g$  towards higher value (see also Table 3) and the decrease in  $\tan \delta$  exhibited by the model PP composites. The model TOCF-reinforced composites exhibited the largest shift in mechanical  $T_g$ ;  $\sim 4$  °C increment over the neat PP, as well as the lowest  $\tan \delta$  value. Model PP composite containing TOCN exhibited only a  $\sim 2$  °C increase in mechanical  $T_g$  over neat PP and higher  $\tan \delta$  value compared to TOCF-reinforced PP composites.

## Conclusions

PP was reinforced with dissolving pulp and TOC of different fibre widths in order to assess their reinforcing potential. It was found that the incorporation of dissolving pulp and the *micrometre-sized* TOCFs into PP led to an improvement in the tensile modulus of the resulting PP/dissolving pulp and PP/TOCF composites by as much as 16% and 35%, respectively, over neat PP. Since wicking measurements showed that both dissolving pulp and TOCFs possessed similar  $\gamma_c$ , the better reinforcing effect of TOCFs can be attributed to the presence of surface microfibrillation on the fibre surface, which led to improved mechanical interlocking and local stiffening of the PP matrix around the fibres, improving the quality of the fibre-matrix interface. The introduction of *nano-sized* TOCN, on the other hand, led to an improvement in the tensile modulus of the resulting PP/TOCN composite by only 10% over neat PP. Whilst no significant changes in the tensile strength of PP/dissolving pulp and PP/TOCFs over unreinforced PP were observed, the incorporation of TOCN into PP led to a decrease in the tensile strength of PP/TOCN. SENB fracture toughness test also showed that PP/TOCN composite possessed lower  $K_{IC}$  value over neat PP. These can be attributed to the agglomeration of TOCN within the PP matrix, which led to earlier onset failure. Our study highlighted the importance of proper dispersion of TOCN in a polymer matrix in order to unleash their potential as *nano-reinforcement* for polymers. The presence of surface microfibrillation on TOCF, on the other hand, increased both the tensile modulus and the SENB fracture toughness of the resulting PP/TOCF composites over neat PP, indicating that *micrometre-sized* TEMPO-oxidised cellulose fibre could also serve as excellent reinforcement for polymers.

**Acknowledgments** We would like to thank Yayasan Khazanah Malaysia for funding A.G.

**Open Access** This article is licensed under a Creative Commons Attribution 4.0 International License, which permits use, sharing, adaptation, distribution and reproduction in any medium or format, as long as you give appropriate credit to the original author(s) and the source, provide a link to the Creative Commons licence, and indicate if changes were made. The images or other third party material in this article are included in the article's Creative Commons licence, unless indicated otherwise in a credit line to the material. If material is not included in the article's Creative Commons licence and your

intended use is not permitted by statutory regulation or exceeds the permitted use, you will need to obtain permission directly from the copyright holder. To view a copy of this licence, visit <http://creativecommons.org/licenses/by/4.0/>.

## References

- Amash A, Zugenmaier P (1998) Study on cellulose and xylan filled polypropylene composites. *Polym Bull* 40:251–258. <https://doi.org/10.1007/s002890050249>
- Araki J, Wada M, Kuga S (2001) Steric stabilization of a cellulose microcrystal suspension by poly(ethylene glycol) grafting. *Langmuir* 17:21–27. <https://doi.org/10.1021/la001070m>
- Bulota M, Vesterinen A-H, Hughes M, Seppälä J (2013) Mechanical behavior, structure, and reinforcement processes of TEMPO-oxidized cellulose reinforced poly(lactic) acid. *Polym Compos* 34:173–179. <https://doi.org/10.1002/pc.22390>
- Chang PS, Robyt JF (1996) Oxidation of primary alcohol groups of naturally occurring polysaccharides with 2,2,6,6-tetramethyl-1-piperidine oxoammonium ion. *J Carbohydr Chem* 15:819–830. <https://doi.org/10.1080/07328309608005694>
- Clarkson CM, Azrak SMEA, Forti ES et al (2020) Recent developments in cellulose nanomaterial composites. *Adv Mater*. <https://doi.org/10.1002/adma.202000718>
- Dietenberger MA, Hasburgh LE (2016) Wood products: thermal degradation and fire. In: Reference module in materials science and materials engineering. Elsevier
- Eichhorn SJ, Davies GR (2006) Modelling the crystalline deformation of native and regenerated cellulose. *Cellulose* 13:291–307. <https://doi.org/10.1007/s10570-006-9046-3>
- Endo R, Saito T, Isogai A (2013) TEMPO-oxidized cellulose nanofibril/poly(vinyl alcohol) composite drawn fibers. *Polymer* 54:935–941. <https://doi.org/10.1016/j.polymer.2012.12.035>
- Fujisawa S, Ikeuchi T, Takeuchi M et al (2012) Superior reinforcement effect of TEMPO-oxidized cellulose nanofibrils in polystyrene matrix: optical, thermal, and mechanical studies. *Biomacromolecules* 13:2188–2194. <https://doi.org/10.1021/bm300609c>
- Fukui S, Ito T, Saito T et al (2018) Counterion design of TEMPO-nanocellulose used as filler to improve properties of hydrogenated acrylonitrile-butadiene matrix. *Compos Sci Technol* 167:339–345. <https://doi.org/10.1016/j.compscitech.2018.08.023>
- Fukui S, Ito T, Saito T et al (2019) Surface-hydrophobized TEMPO-nanocellulose/rubber composite films prepared in heterogeneous and homogeneous systems. *Cellulose* 26:463–473. <https://doi.org/10.1007/s10570-018-2107-6>
- Fukuzumi H, Saito T, Iwata T et al (2009) Transparent and high gas barrier films of cellulose nanofibers prepared by TEMPO-mediated oxidation. *Biomacromolecules* 10:162–165. <https://doi.org/10.1021/bm801065u>
- Fukuzumi H, Saito T, Okita Y, Isogai A (2010) Thermal stabilization of TEMPO-oxidized cellulose. *Polym Degrad Stab*

- 95:1502–1508. <https://doi.org/10.1016/j.polymdegradstab.2010.06.015>
- Gee DR, Melia TP (1970) Thermal properties of melt and solution crystallized isotactic polypropylene. *Die Makromolekulare Chemie* 132:195–201. <https://doi.org/10.1002/macp.1970.021320117>
- Geng S, Wei J, Aitomäki Y et al (2018) Well-dispersed cellulose nanocrystals in hydrophobic polymers by in situ polymerization for synthesizing highly reinforced biocomposites. *Nanoscale* 10:11797–11807. <https://doi.org/10.1039/C7NR09080C>
- Gray DG (2008) Transcrystallization of polypropylene at cellulose nanocrystal surfaces. *Cellulose* 15:297–301. <https://doi.org/10.1007/s10570-007-9176-2>
- Greenhalgh E (2009) Failure analysis and fractography of polymer composites. Elsevier, Amsterdam
- Grundke K, Bogumil T, Gietzelt T et al (1996) Wetting measurements on smooth, rough and porous solid surfaces. In: Interfaces, surfactants and colloids in engineering. Steinkopff, pp 58–68
- Hietala M, Rollo P, Kekäläinen K, Oksman K (2014) Extrusion processing of green biocomposites: compounding, fibrillation efficiency, and fiber dispersion. *J Appl Polym Sci*. <https://doi.org/10.1002/app.39981>
- Hull D (1999) Fractography: observing, measuring and interpreting fracture surface topography. Cambridge University Press, Cambridge
- Hull D, Clyne TW (1996) An introduction to composite materials. Cambridge University Press, Cambridge
- Isogai A, Kato Y (1998) Preparation of polyuronic acid from cellulose by TEMPO-mediated oxidation. *Cellulose* 5:153–164. <https://doi.org/10.1023/A:1009208603673>
- Johnson RK, Zink-Sharp A, Rennecker SH, Glasser WG (2009) A new bio-based nanocomposite: fibrillated TEMPO-oxidized celluloses in hydroxypropylcellulose matrix. *Cellulose* 16:227–238. <https://doi.org/10.1007/s10570-008-9269-6>
- Kurihara T, Isogai A (2014) Properties of poly(acrylamide)/TEMPO-oxidized cellulose nanofibril composite films. *Cellulose* 21:291–299. <https://doi.org/10.1007/s10570-013-0124-z>
- Lee K-Y, Bharadia P, Blaker JJ, Bismarck A (2012) Short sisal fibre reinforced bacterial cellulose polylactide nanocomposites using hairy sisal fibres as reinforcement. *Compos Part Appl Sci Manuf* 43:2065–2074. <https://doi.org/10.1016/j.compositesa.2012.06.013>
- Lee K-Y, Aitomäki Y, Berglund LA et al (2014) On the use of nanocellulose as reinforcement in polymer matrix composites. *Compos Sci Technol* 105:15–27. <https://doi.org/10.1016/j.compscitech.2014.08.032>
- Lichtenstein K, Lavoine N (2017) Toward a deeper understanding of the thermal degradation mechanism of nanocellulose. *Polym Degrad Stab* 146:53–60. <https://doi.org/10.1016/j.polymdegradstab.2017.09.018>
- Luner P, Sandell M (1969) The wetting of cellulose and wood hemicelluloses. *J Polym Sci Part C Polym Symp* 28:115–142. <https://doi.org/10.1002/polc.5070280112>
- Mamleev V, Bourbigot S, Yvon J (2007) Kinetic analysis of the thermal decomposition of cellulose: the main step of mass loss. *J Anal Appl Pyrolysis* 80:151–165. <https://doi.org/10.1016/j.jaap.2007.01.013>
- Mautner A, Lee K-Y, Lahtinen P et al (2014) Nanopapers for organic solvent nanofiltration. *Chem Commun* 50:5778–5781. <https://doi.org/10.1039/C4CC00467A>
- Mautner A, Lee K-Y, Tammelin T et al (2015) Cellulose nanopapers as tight aqueous ultra-filtration membranes. *React Funct Polym* 86:209–214. <https://doi.org/10.1016/j.reactfunctpolym.2014.09.014>
- Noguchi T, Endo M, Niihara K et al (2020) Cellulose nanofiber/elastomer composites with high tensile strength, modulus, toughness, and thermal stability prepared by high-shear kneading. *Compos Sci Technol* 188:108005. <https://doi.org/10.1016/j.compscitech.2020.108005>
- Paukkeri R, Lehtinen A (1993) Thermal behaviour of polypropylene fractions: 2. The multiple melting peaks. *Polymer* 34:4083–4088. [https://doi.org/10.1016/0032-3861\(93\)90670-6](https://doi.org/10.1016/0032-3861(93)90670-6)
- Petersson L, Kvien I, Oksman K (2007) Structure and thermal properties of poly(lactic acid)/cellulose whiskers nanocomposite materials. *Compos Sci Technol* 67:2535–2544. <https://doi.org/10.1016/j.compscitech.2006.12.012>
- Sacui IA, Nieuwendaal RC, Burnett DJ et al (2014) Comparison of the properties of cellulose nanocrystals and cellulose nanofibrils isolated from bacteria, tunicate, and wood processed using acid, enzymatic, mechanical, and oxidative methods. *ACS Appl Mater Interfaces* 6:6127–6138. <https://doi.org/10.1021/am500359f>
- Saito T, Isogai A (2004) TEMPO-mediated oxidation of native cellulose. The effect of oxidation conditions on chemical and crystal structures of the water-insoluble fractions. *Biomacromolecules* 5:1983–1989. <https://doi.org/10.1021/bm0497769>
- Saito T, Nishiyama Y, Putaux J-L et al (2006) Homogeneous suspensions of individualized microfibrils from TEMPO-catalyzed oxidation of native cellulose. *Biomacromolecules* 7:1687–1691. <https://doi.org/10.1021/bm060154s>
- Saito T, Kimura S, Nishiyama Y, Isogai A (2007) Cellulose nanofibers prepared by TEMPO-mediated oxidation of native cellulose. *Biomacromolecules* 8:2485–2491. <https://doi.org/10.1021/bm0703970>
- Saito T, Kuramae R, Wohlert J et al (2013) An ultrastrong nanofibrillar biomaterial: the strength of single cellulose nanofibrils revealed via sonication-induced fragmentation. *Biomacromolecules* 14:248–253. <https://doi.org/10.1021/bm301674e>
- Santmartí A, Lee K-Y (2018) Crystallinity and thermal stability of nanocellulose. In: Lee K-Y (ed) *Nanocellulose and sustainability*, 1st edn. CRC Press, Boca Raton, pp 67–86
- Soeta H, Lo Re G, Masuda A et al (2018) Tailoring nanocellulose–cellulose triacetate interfaces by varying the surface grafting density of poly(ethylene glycol). *ACS Omega* 3:11883–11889. <https://doi.org/10.1021/acsomega.8b01616>
- Szekely J, Neumann AW, Chuang YK (1971) The rate of capillary penetration and the applicability of the Washburn equation. *J Colloid Interface Sci* 35:273–278. [https://doi.org/10.1016/0021-9797\(71\)90120-2](https://doi.org/10.1016/0021-9797(71)90120-2)
- Takaichi S, Saito T, Tanaka R, Isogai A (2014) Improvement of nanodispersibility of oven-dried TEMPO-oxidized

- celluloses in water. *Cellulose* 21:4093–4103. <https://doi.org/10.1007/s10570-014-0444-7>
- Tröger J, Lunkwitz K, Grundke K, Bürger W (1998) Determination of the surface tension of microporous membranes using wetting kinetics measurements. *Colloids Surf Physicochem Eng Asp* 134:299–304. [https://doi.org/10.1016/S0927-7757\(97\)00158-1](https://doi.org/10.1016/S0927-7757(97)00158-1)
- Wang S, Lin Y, Zhang X, Lu C (2015) Towards mechanically robust cellulose fiber-reinforced polypropylene composites with strong interfacial interaction through dual modification. *RSC Adv* 5:50660–50667. <https://doi.org/10.1039/C5RA01792K>
- Wang Z, Qiao X, Sun K (2018) Rice straw cellulose nanofibrils reinforced poly(vinyl alcohol) composite films. *Carbohydr Polym* 197:442–450. <https://doi.org/10.1016/j.carbpol.2018.06.025>
- Ye D, Farriol X (2005) Improving accessibility and reactivity of celluloses of annual plants for the synthesis of methylcellulose. *Cellulose* 12:507–515. <https://doi.org/10.1007/s10570-005-7133-5>
- Zisman WA (1964) Relation of the equilibrium contact angle to liquid and solid constitution. In: Fowkes FM (ed) *Contact angle, wettability, and adhesion*. American Chemical Society, Washington, pp 1–51

**Publisher's Note** Springer Nature remains neutral with regard to jurisdictional claims in published maps and institutional affiliations.